Received: 23 February 2022 | Accepted: 21 December 2022

DOI: 10.1002/jcp.30940

RESEARCH ARTICLE

Journal of Cellular Physiology WILEY

Cyclo-glycylproline attenuates hydrogen peroxide-induced cellular damage mediated by the MDM2-p53 pathway in human neural stem cells

Kazutoshi Murotomi[1] | Harumi Kagiwada[2] | Kazumi Hirano[1] | Shoko Yamamoto[3] | Noriaki Numata[3] | Yo Matsumoto[3] | Hidekazu Kaneko[4] | Masakazu Namihira[1]

[1]Molecular Neurophysiology Research Group, Biomedical Research Institute, National Institute of Advanced Industrial Science and Technology (AIST), Tsukuba, Japan

[2]Biological Data Science Research Group, Cellular and Molecular Biotechnology Research Institute, National Institute of Advanced Industrial Science and Technology (AIST), Tokyo, Japan

[3]Technical Center, Jellice Co., Ltd., Miyagi, Tagajo, Japan

[4]Neurorehabilitation Research Group, Human Informatics and Interaction Research Institute, National Institute of Advanced Industrial Science and Technology (AIST), Tsukuba, Japan

Correspondence

Masakazu Namihira and Kazutoshi Murotomi, Biomedical Research Institute, National Institute of Advanced Industrial Science and Technology (AIST), 1-1-1 Higashi, Tsukuba 305-8566, Ibaraki, Japan.
Email: m-namihira@aist.go.jp and k-murotomi@aist.go.jp

Funding information

Japan Society for the Promotion of Science; New Energy and Industrial Technology Development Organization

Abstract

Cyclo-glycylproline (cGP), a cyclic dipeptide containing a condensation bond between glycine and proline, is produced by the cyclization of the N-terminal tripeptide of insulin-like growth factor-1. Previous studies have shown that cGP administration exerts a neuroprotective effect and enhances the regenerative ability in rats with ischemic brain injury. The efficacy of cGP is medicated by regulating the bioavailability of insulin-like growth factor-1 (IGF-1), however, the molecular mechanisms underlying the neuroprotective effects of cGP on brain damage remains to be elucidated. In the current study, we investigated the cGP-mediated molecular mechanism in human fetal neural stem cells (hfNSCs) exposed to oxidative stress, which is a key factor affecting the development of several brain diseases, including traumatic brain injury and Parkinson's disease. We found that cGP treatment attenuated oxidative stress-induced cell death in cultured hfNSCs in a dose-dependent manner. Transcriptome analysis revealed that under oxidative stress conditions, p53-mediated signaling was activated, accompanied by upregulation of mouse double minute 2 homolog (MDM2), a p53-specific E3 ubiquitin ligase, in cGP-treated hfNSCs. By using a comprehensive protein phosphorylation array, we found that cGP induced the activation of Akt signaling pathway, which enhanced the expression of MDM2, in hfNSCs exposed to oxidative stress. Moreover, the MDM2 inhibitor nutlin-3 inhibited the protective effect of cGP on oxidative stress-induced cell death and apoptosis. Therefore, cGP attenuates oxidative stress-induced cell death mediated by the interplay between IGF-1 signaling and the MDM2-p53 pathway in human NSCs. We revealed the molecular mechanism underlying cGP-induced neuroprotective properties in a model of brain damage.

KEYWORDS

cyclic peptide, cyclo-glycylproline, MDM2, neural stem cell, neuroprotection, oxidative stress, p53

1 | INTRODUCTION

Oligopeptides, which consist of two or more amino acids, are transported across the blood-brain barrier (Smith et al., 2004) and function as neurotransmitters and neuromodulators (Rehm et al., 2008). Certain peptides can ameliorate ischemic brain injury and Parkinson's disease owing to their antioxidant and anti-inflammatory effects in neurons and glial cells (Boldyrev et al., 2013; Korkmaz and Tunçel, 2018). For instance, cyclo-glycylproline (cGP), a cyclic dipeptide containing a condensation bond between glycine and proline, may exert neuroprotective effects against cerebral ischemia. cGP present in human plasma and cerebrospinal fluid (Fan et al., 2018, 2019) is produced by cyclization of the N-terminal tripeptide of insulin-like growth factor-1 (IGF-1) to form glycine-proline-glutamate (Nilsson-Håkansson et al., 1993). It has been reported that external treatment of rats with cGP prevents brain damage and retains spatial memory function in ischemic brain injury (Guan et al., 2007; Ostrovskaya et al., 1999). In addition, oral administration of cGP facilitates the rehabilitation process by enhancing neural plasticity in rats with focal ischemic infarction (Kaneko et al., 2022). As cGP also exhibits antiamnestic activity (Gudasheva et al., 1996), anxiolytic effects (Gudasheva et al., 2020), and retention of memory (Ostrovskaya et al., 1999) by regulating several aspects of neuronal functions, cGP may represent a promising peptide for improving brain function under physiological and pathological conditions.

cGP can bind to IGF-1-binding protein 3 (IGFBP-3) (Guan et al., 2014), which regulates the homeostasis of IGF-1 by binding to circulating IGF-1 (Jogie-Brahim et al., 2009). It has been suggested that cGP modulates the IGF-1 signaling pathway by regulating bioavailability of IGF-1, which provides neuroprotective effects against ischemic brain damage (Serhan et al., 2020) and β-amyloid-induced neural death (Aguado-Llera et al., 2018), mediated by the regulation of bioavailable IGF-1 (Fan et al., 2018). cGP also induces an increase in brain-derived neurotropic factor levels (Gudasheva et al., 2016) and ionic currents via the GABA receptor (Sharonova et al., 2019), which provide protection against neuronal death in cerebral ischemic stroke (Schwartz-Bloom & Sah, 2001). These findings suggest that the activation of IGF-1 signaling and increase in brain-derived neurotropic factor levels represent one of the mechanisms underlying the cGP-mediated neuroprotective effect against ischemic brain injury. However, the downstream molecular mechanisms that cGP-induced regulation of bioavailable IGF-1 in brain damage remains unclear. Additionally, the neurotrophin-like activity of cGP in human neural cells has not yet been examined.

Recent studies have shown that human neural stem cells, which can differentiate into neurons, astrocytes, and oligodendrocytes, are valuable for screening therapeutic and toxic agents to identify factors affecting the human brain (Patnaik & Padhy, 2017). Therefore, in the present study, we investigated the cGP-mediated molecular mechanism in human fetal neural stem cells (hfNSCs) exposed to oxidative stress, which induces brain damage during the development of several brain diseases, including ischemic stroke, traumatic brain injury, and Parkinson's disease (Navarro-Yepes et al., 2014). We identified a novel molecular mechanism for the protective effect of cGP against brain damage.

2 | MATERIALS AND METHODS

2.1 | hfNSC culture

hfNSCs were purchased from PhoenixSongs Biologicals, Inc. The cell line was derived from a human cerebral cortex from a male fetus at embryonic week 14. The cells were seeded into culture dishes or plates coated with poly-L-ornithine (Sigma-Aldrich) and laminin (Corning, Inc.) and cultured in N2-supplemented Dulbecco's modified Eagle medium/nutrient mixture F-12 (DMEM/F-12; Thermo Fisher Scientific) containing 0.1% B27 supplement (Thermo Fisher Scientific), 10 ng/ml human recombinant basic fibroblast growth factor (Wako Pure Chemical Industries), and 20 ng/ml human recombinant epidermal growth factor (Wako Pure Chemical Industries) in a humidified atmosphere containing 5% CO_2 at 37°C. All experiments involving human cells were approved by the Committee for the Ethics on the Experiments with Human Derivative Samples of the National Institute of Advanced Industrial Science and Technology.

For neuronal differentiation, hfNSCs were cultured in neurobasal medium (Thermo Fisher Scientific) containing 2% B27 supplement and GlutaMAX (Invitrogen) for 7 days. For astrocyte differentiation, hfNSCs were cultured in N2-supplemented DMEM/F-12 containing 10 ng/ml leukemia inhibitory factor for 3 days. To measure the differentiation rate, the cells were washed with phosphate-buffered saline (PBS), fixed in 4% paraformaldehyde (PFA) in PBS, and stained with βIII-tubulin (Tuj-1, 1:400 dilution; R&D Systems) or GFAP (1:500 dilution; Cell Signaling Technologies) antibodies. Nuclei were stained with Hoechst 33342 (Dojindo Laboratories). Stained cells were visualized using a fluorescence microscope (BX53; Olympus), and the differentiation rate was calculated as the ratio of Tuj-1- or GFAP-positive cells to Hoechst-positive cells.

To analyze apoptotic cells, hfNSCs were seeded into a 35 mm-dish (Nunc; Thermo Fisher Scientific). After overnight incubation, hydrogen peroxide (H_2O_2) and cGP were added to the hfNSCs for 12 h and the cells were stained with antibodies against active caspase-3 (1:250 dillution; R&D Systems) and nestin (1:500 dilution; Abcam). The nuclei were stained with Hoechst 33342. The apoptotic cells were calculated as the ratio of active caspase-3-positive cells to Hoechst-positive cells.

2.2 | Measurement of cell viability

hfNSCs were plated into a 96-well microplate (Nunc; Thermo Fisher Scientific) and incubated overnight at 37°C with 5% CO_2. Culture medium containing 100 μM H_2O_2 and different concentrations of cGP, which was synthesized by Bachem Japan K. K. and dissolved in PBS, was added to the microplate at 100 μl/well for 8 h. In the case of the SH-SY5Y neuroblastoma cell line, 300 μM H_2O_2 and different

concentrations of cGP were added to the cells for 24 h. After incubation at 37°C with 5% CO_2, Cell Counting Kit-8 (Dojindo Laboratories) reagent was added to each well and the absorbance was measured at 450 nm. Cell viability was calculated relative to the absorbance of control cells set at 100%.

2.3 | Measurement of cell proliferation rate

hfNSCs were plated into a 35 mm-dish (Nunc; Thermo Fisher Scientific) and incubated overnight at 37°C with 5% CO_2. Visualization of proliferative cells was performed using a Click-iT EdU Cell Proliferation Kit (Thermo Fisher Scientific) according to the manufacturer's instructions. Briefly, 2.5 μM 5-ethynyl-2′-deoxyuridine (EdU) was added to the cells for 2 h, after which the cells were fixed in 4% PFA. After the Click-iT reaction, the nuclei were stained with Hoechst 33342. Stained cells were visualized using a fluorescence microscope (THUNDER Imaging Systems; Leica Microsystems), and the rate of cell proliferation was calculated by dividing EdU-positive cells (green) by Hoechst-positive cells (blue).

2.4 | Measurement of antioxidant capacity

The antioxidant capacity of the cGP solutions was measured using a 2,2-diphenyl-1-picrylhydrazyl (DPPH) antioxidant assay kit (Dojindo Laboratories) according to the manufacturer's instructions. A vitamin E analog, 6-hydroxy-2,5,7,8-tetramethylchroman-2-carboxylic acid (Trolox), was used as a positive control.

2.5 | RNA-seq analysis

RNA was extracted from the cells using TRIzol reagent (Invitrogen) according to the manufacturer's instructions. RNA-seq was performed at Macrogen Japan Corp. Three independent samples were assayed to evaluate the reproducibility of the experimental procedures. The quantity and integrity of total RNA (2 μg) were evaluated using an Agilent Bioanalyzer (Agilent Technologies). All samples provided for sequencing, except for H_2O_2-treated cells, had an RNA integrity number >7.0. A sequencing library was prepared using the TruSeq Stranded messenger RNA (mRNA) Library Prep kit (Illumina) according to the manufacturer's instructions. The libraries for RNA sequencing were sequenced using Illumina Sequencing by Synthesis chemistry with 2 × 100-bp paired-end reads on a NovaSeq6000 (Illumina). The obtained sequencing data were analyzed using an open bioinformatics tool for quick analysis of RNA-seq data, RaNA-seq (Prieto & Barrios, 2019). In the pipeline, the FASTQ files were preprocessed using the Fastp tool (Chen et al., 2018), and the expression was quantified using Salmon (Patro et al., 2017). The quality of raw data was represented in graphs produced using the package RJSplot (Barrios & Prieto, 2018), and the distances between plots in the graphs were calculated using SERE (Schulze et al., 2012). DEseq2 (Love et al., 2014) was used to identify differentially expressed genes (DEGs) with more than twofold-changes in transcripts per million between the control and cGP, H_2O_2, or H_2O_2 + cGP-treated groups. Enrichment analysis based on the DEGs (fold-change > 2.0, $p < 0.05$ in Wald test) was performed using the Reactome pathways database (Jassal et al., 2020) in the PANTHER Classification System.

2.6 | Quantitative PCR

Total RNA (2 μg) was used as a template for complementary DNA synthesis, which was performed using SuperScript IV VILO (Invitrogen). Gene expression was analyzed using KOD SYBR qPCR Mix (Toyobo) and a CFX Connect Real-Time System (Bio-Rad). The primers used are listed in Table S1. The cycling conditions were as follows: initial denaturation at 95°C for 30 s, followed by 40 cycles of 95°C for 5 s and 60°C for 30 s. Subsequently, the melting curve was analyzed over a linear temperature gradient from 65°C to 95°C to assess whether a single PCR product was synthesized. Relative gene expression levels were determined after normalization to the corresponding sample expression levels of 18S ribosomal RNA.

2.7 | Analysis of active signaling pathway using phosphorylation protein array

A phosphorylation protein array was used as previously described (Kagiwada et al., 2021). At 4 h after H_2O_2 and cGP treatment, the hfNSCs were washed with ice-cold PBS and lysed with M-PER (Thermo Fisher Scientific) containing a protease inhibitor cocktail. The protein content in the lysates was measured using a BCA protein assay kit (Takara Bio), and 80 μg protein was applied to a protein array of 1,200 proteins loaded on a GST/GSH-coated glass slide. After the kinase reaction and detection of phosphorylated proteins on the array, phosphorylation levels were compared between the nontreated control and H_2O_2- and/or cGP-treated samples using the rank product test (Breitling et al., 2004). All p-values <0.05, with increased phosphorylation levels, were considered as statistically significant. The probability of each pathway was estimated based on the hypergeometric distribution for the 376 pathways.

2.8 | Western immunoblotting

The cell lysates were prepared using the aforementioned method in phosphorylation protein array section, and the samples were incubated with sample buffer (Nacalai Tesque) for 5 min at 95°C. Aliquots of the samples were separated using 5%–20% SuperSep (Wako Pure Chemical Industries) and transferred onto polyvinylidene fluoride membranes (EMD Millipore). After blocking with Bullet Blocking One (Nacalai Tesque), the membranes were incubated with the appropriate primary antibodies at 4°C. The membranes were washed with Tris-buffered saline containing 0.1% Tween 20 and incubated with the appropriate horseradish peroxidase-conjugated

secondary antibodies (Cell Signaling Technology). The bound antibody was detected using ECL Prime reagents (GE Healthcare Bio-Sciences). Immunoblots were semi-quantified using computerized densitometry and an image analyzer (Image Stadio Software; SCRUM, Inc.).

2.9 | Statistical analysis

The results are expressed as the mean ± standard error (*SE*). Statistical analysis was performed via analysis of variance followed by Tukey's test for multiple comparisons and Mann–Whitney *U* test for nonparametric comparisons using Ekuseru-Toukei 2012 software and GraphPad Prism ver. 9 (Dotmatics).

3 | RESULTS

3.1 | Effect of cGP on hydrogen peroxide-induced death of hfNSCs

To determine whether cGP exerts protective effects against oxidative damage in hfNSCs, we measured the viability of cGP-treated cells after treatment with hydrogen peroxide (H_2O_2), which is used to simulate oxidative stress conditions in cultured cells. H_2O_2-induced cell death was attenuated by treatment with cGP in a dose-dependent manner, and treatment with >100 nM cGP considerably inhibited the reduction in cell viability after H_2O_2 treatment (Figure 1). Pretreatment with 1 mM cGP for 2 h had no effect on viability in H_2O_2-treated hfNSCs (Figure S1a). Treatment with more than 1 μM cGP also significantly attenuated H_2O_2-induced cell death in SH-SY5Y cells (Figure S1b). Although the proliferation rate of H_2O_2-treated hfNSCs could not be measured accurately because the H_2O_2-treated hfNSCs had damaged and aggregated nuclei, the addition of cGP at least prevented H_2O_2-expossed cell damage with maintained cell proliferative capacity (Figure S2). The DPPH-radical scavenging ratio of cGP (10 μM–10 mM) was 0.06%–0.6%, whereas that of Trolox (positive control) was 25.5%, indicating that cGP had no antioxidant capacity (Figure S3). These results indicate that cGP prevents oxidative stress-induced cell death in hfNSCs without direct radical-scavenging activity. Additionally, cGP had no effect on the differentiation of hfNSCs into astrocytes and neurons (Figure S4). As the protective effect of cGP against oxidative stress was in a dose-dependent manner, the highest concentration (1 mM) of cGP was used throughout subsequent experiments.

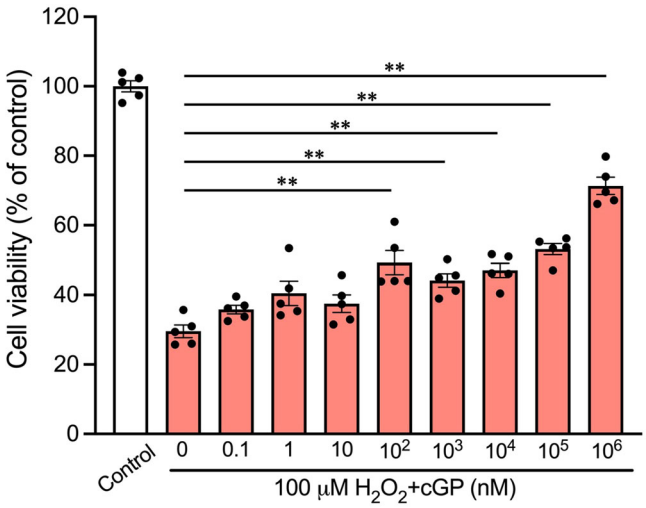

FIGURE 1 Viability of hfNSCs after treatment with H_2O_2 and cGP. Cells were treated with H_2O_2 (100 μM) and cGP (0.1 nM–1 mM) for 8 h. The results are presented as the mean ± *SE* ($n = 5$), and black dots indicate individual values in the group. Statistical analyses were carried out using analysis of variance (Tukey's test). Cells treated without H_2O_2 and cGP were used as controls. $^{**}p < 0.01$ compared with control. cGP, cyclo-glycylproline; hfNSCs, human fetal neural stem cells; H_2O_2, hydrogen peroxide

3.2 | Analysis of global gene expression in H_2O_2- and cGP-treated hfNSCs

To elucidate the potential mechanism of cGP in preventing oxidative damage in NSCs, we performed comprehensive gene expression analysis using RNA-seq. All DEGs (a, 24,039; b, 23,839) were visualized using Volcano plots for H_2O_2 treatment of hfNSCs for 8 h. H_2O_2 treatment considerably upregulated (>2-fold) 259 genes and downregulated (<0.5-fold) 698 genes in hfNSCs (Figure 2a). To visualize the biological response after H_2O_2 treatment, the genes were sorted according to the Reactome pathway. The enriched pathways in upregulated genes included TP53-mediated transcription, which is triggered by various external stress stimuli (Figure S5a); enriched pathways in downregulated genes included a gene cluster related to neuronal functions, such as protein-protein interactions at synapses, neuronal system, and axon guidance (Figure S5b). In enrichment analysis using the Reactome pathway database, addition of cGP with H_2O_2 upregulated various gene exprssion (transcription), including transcriptional regulation by TP53 compared to treatment of H_2O_2 alone (Figure S5c). Genes associated with the cell cycle were downregulated following cGP treatment (Figure S5d). Treatment with cGP alone altered the expression of only 14 genes in hfNSCs (Figure S5e), whereas co-treatment with cGP and H_2O_2 significantly altered the expression of >500 genes compared to that obtained via treatment with H_2O_2 alone (Figure 2b). To identify the group of genes regulated via cGP treatment, we focused on the upregulated and downregulated genes only in the H_2O_2 + cGP treatment group. For the 223 upregulated genes, we observed significant enrichments in external stress-induced signals, including TP53 and p38MAPK (Figure 2c). In contrast, cell cycle-associated genes were significantly enriched in downregulated genes following treatment with H_2O_2 + cGP (Figure 2d).

To validate the results of whole-transcriptome RNA-seq, the expression levels of genes related to p53 and the cell cycle were evaluated using quantitative PCR. The expression levels of some p53

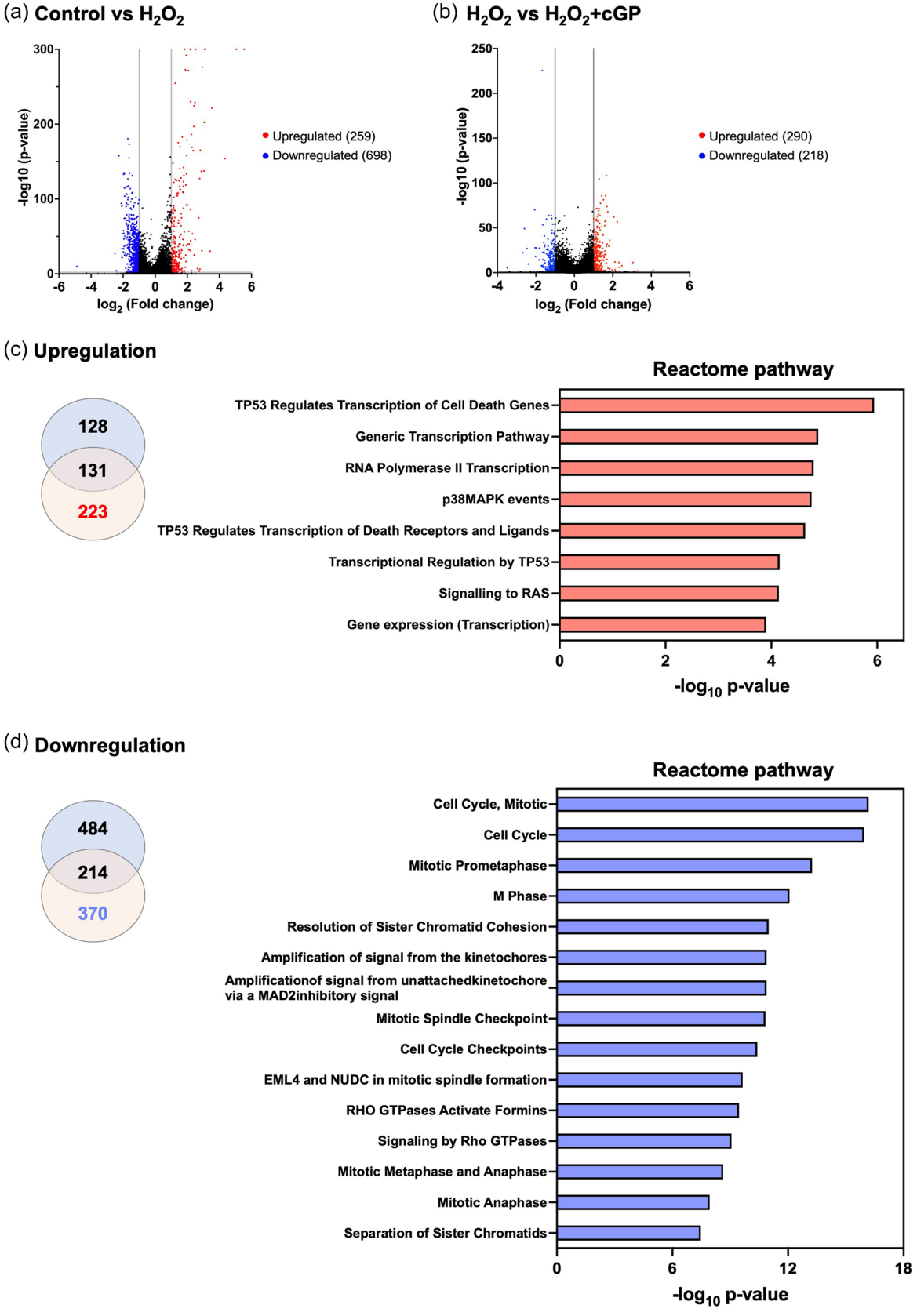

FIGURE 2 (See caption on next page)

pathway-related genes, such as *TP53I3*, *PIDD1*, *TNFRSF10B*, and *p21*, in H_2O_2-treated hfNSCs were significantly higher than those in control cells (Figure 3a). Consistent with the results of RNA-seq analysis, the expression of upregulated genes induced by activation of the p53 pathway, including mouse double minute 2 homolog (*MDM2*), *TP53I3*, *PIDD1*, *TNFRSF10B*, *ZMAT3*, and *p21*, in H_2O_2 + cGP-treated cells were considerably increased compared to that in H_2O_2-treated cells alone (Figure 3a). In contrast, the expression levels of some cell cycle-associated genes, such as *CDC20*, *CCNB1*, and *CCNB2*, in H_2O_2-treated hfNSCs were 1.2–1.4-fold higher than those in control cells (Figure 3b). The gene expression of cell cycle-associated genes, such as *CDC20*, *CCNB1*, *CCNB2*, *CENPA*, and *EHMT2*, in H_2O_2 + cGP-treated cells was considerably decreased compared to that in H_2O_2-treated cells, which agreed with the RNA-seq results (Figure 3b). p53 protein levels in H_2O_2 + cGP-treated hfNSCs for 4 h were significantly increased compared with those in

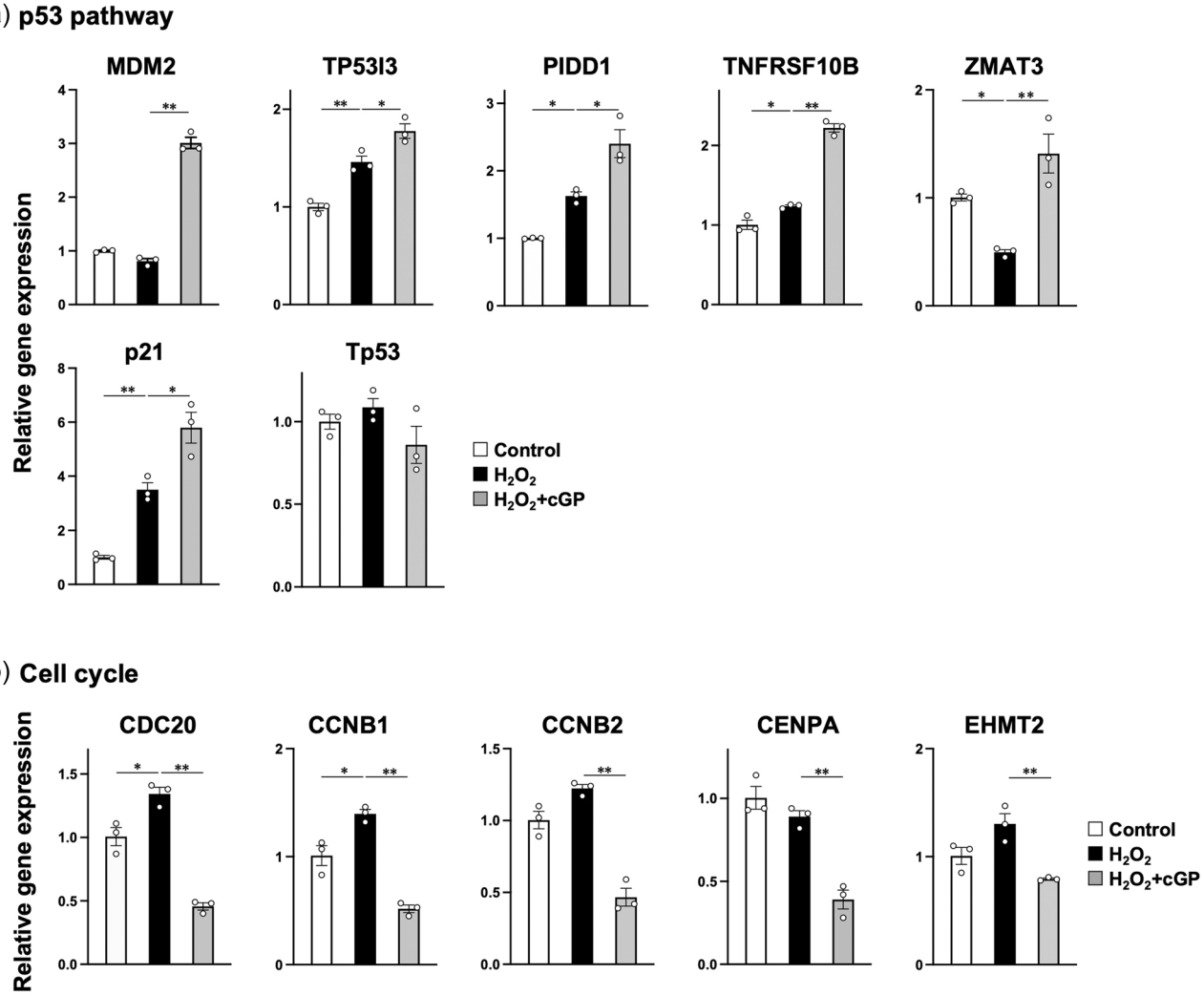

FIGURE 3 Gene expression associated with the p53 pathway and cell cycle in hfNSCs after treatment with H_2O_2 and cGP. The expression levels of p53-related (a: MDM2, TP53I3, PIDD1, TNFRSF10B, ZMAT3, p21, and Tp53) and cell cycle-associated (b: CDC20, CCNB1, CCNB2, CENPA, and EHMT2) genes were measured at 8 h after treatment with H_2O_2 and 1 mM cGP. Results are expressed as values (mean ± *SE*) relative to the control ($n = 3$ each). Statistical analyses were carried out using analysis of variance (Tukey's test). $^*p < 0.05$; $^{**}p < 0.01$. cGP, cyclo-glycylproline; hfNSCs, human fetal neural stem cells; H_2O_2, hydrogen peroxide

FIGURE 2 Transcriptomic and enrichment analyses in hfNSCs treated with 100 μM H_2O_2 and 1 mM cGP for 8 h. (a, b) Volcano plots indicating -log10 *p*-value in relation to the log2 scaled fold-change for the (a) control versus H_2O_2 treatment and (b) H_2O_2 versus H_2O_2 + cGP treatment. Genes that passed the significance threshold false discovery rate adjusted *p*-value <0.05 and expression cut-off $\log_2$ (fold-change) >1. 0 and <−1.0 are indicated in red and blue, respectively. (c, d) Venn diagram indicating the numbers of (c) upregulated and (d) downregulated DEGs identified by comparing the control and H_2O_2 or H_2O_2 + cGP treatments. In total, 223 genes (red) were upregulated, and 370 genes (blue) were downregulated in only the H_2O_2 + cGP treatment group; these genes were enriched in the Reactome pathway in the PANTHER Classification System. cGP, cyclo-glycylproline; hfNSCs, human fetal neural stem cells; H_2O_2, hydrogen peroxide

H_2O_2-treated cells (Figure S6). These results suggest that cGP induces the additional increase in p53 protein after the addition of H_2O_2, resulting in upregulation of *TP53I3*, *MDM2*, and *p21* expression levels compared to the cells treated with H_2O_2 (Figure 3a). Given that activation of the p53 pathway induces cell cycle arrest and apoptosis (Chen, 2016), our gene expression analyses indicate that cGP treatment may promote the activation of the p53 pathway and subsequent downregulation of cell cycle-associated gene expression under oxidative stress conditions in hfNSCs.

Although the p53 pathway was activated in H_2O_2-treated hfNSCs in GO analysis (Figure S5a), the degree of activation of p53 signaling in H_2O_2-treated cells was not higher than that in H_2O_2- and cGP-treated cells (Figure S6). The mild activation of p53 signaling may not contribute to downregulating cell cycle-related genes that were not included in the group of downregulated genes in H_2O_2-treated cells in the enrichment analysis (Figure S5b). RT-qPCR analysis revealed that the cell cycle-related gene expression levels in the H_2O_2-treated group were significantly higher than those in the control group, but the degree of increase was observed to be only 1.2–1.4-fold (Figure 3b). These results suggest that the effect of oxidative stress on the cell cycle in hfNSCs may be mild since the activity of the p53 pathway in these cells is only slightly higher under the oxidative stress conditions.

3.3 | cGP-induced signal transduction pathway in hfNSCs

cGP has been reported to promote the activation of tyrosine phosphorylation of the IGF-1 receptors in rat brain (Guan et al., 2014) and inhibiting in mammary gland (Singh-Mallah et al., 2017), and protein phosphorylation regulates the activity of the p53 signaling pathway (Maclaine & Hupp, 2009). Therefore, we used a comprehensive protein phosphorylation array to investigate whether cGP affects the activation of intracellular signaling pathways via protein phosphorylation in hfNSCs (Figure 4a). The active pathways based on rank product analysis ($p < 0.05$) in hfNSCs after H_2O_2 + cGP treatment are indicated by colored and yellow lines and are listed in a table in Figure S7. This array revealed that the epidermal growth factor signal was significantly activated from the receptor and nuclear transcription in H_2O_2 + cGP (Figure S7). The activated pathways in H_2O_2 + cGP-treated cells were included in the mitogen-activated protein kinase 6 (MAPK6)-MAPK4 (extracellular signal-regulated kinase 3 [ERK3]-ERK4) and phosphoinositide 3-kinase-protein kinase B (Akt) signaling pathways (Figure S7). The subtracted fluorescence intensity of the pathway comprising proteins, such as CDC14A, CDKN1B, and MAPKAPK5, in H_2O_2 + cGP-treated cells was significantly increased compared to that in H_2O_2-treated cells (Figure 4b). Western blotting analysis similarly showed that the ratio of phosphorylated ERK and Akt in H_2O_2 + cGP-treated cells was significantly increased compared to that in H_2O_2-treated cells (Figure 4c,d). The ratio of pERK in H_2O_2 + cGP-treated cells was similar to that in the control (Figure 4c), suggesting that treatment of hfNSCs with H_2O_2 suppresses the activity of the MAPK pathway, and cGP may prevent the inactivation of its pathway. The levels of phosphorylated Akt in the H_2O_2 + cGP treatment group were considerably increased compared to those in the H_2O_2 treatment group (Figure 4d). These results suggest that cGP not only contributes to the maintenance of MAPK but also activates Akt-mediated signals in NSCs exposed to oxidative stress.

3.4 | Effect of an MDM2 inhibitor on the protective effect of cGP against oxidative stress-induced cell death

cGP treatment induced the expression of *MDM2*, the principal cellular antagonist of p53 (Moll & Petrenko, 2003), suggesting that cGP inhibits excessive activation of the p53 pathway via upregulation of MDM2 in hfNSCs exposed to oxidative stress. To test this hypothesis, we investigated the effect of the MDM2 inhibitor nutlin-3 on H_2O_2-induced cell death in hfNSCs. The expression level of p21, a p53-dependent transcriptional factor, after nutlin-3 treatment was significantly increased in control cells and H_2O_2 + cGP-treated hfNSCs (Figure S8), suggesting that upregulated MDM2 by cGP contributes to regulating the transcriptional activation of p53. Treatment with nutlin-3 alone had no effect on the decrease in viability of H_2O_2-treated hfNSCs (Figure 5). Although cGP treatment prevented the H_2O_2-induced decrease in the viability of hfNSCs, treatment with nutlin-3 considerably reduced cell viability, even in the presence of cGP, in a concentration-dependent manner. These results demonstrate that the protective effects of cGP on oxidative stress-induced cell death in hfNSCs is mediated by MDM2 activation.

Furthermore, to reveal the involvement of MDM2 in cell apoptosis, we analyzed apoptosis in hfNSCs in the absence or presence of the MDM2 inhibitor nutlin-3 using an antibody against active caspase-3, a marker for apoptotic cells. As shown in Figure S9, the rate of active caspase-3-positive cells was significantly increased with H_2O_2 treatment, and the increase in active capsase-3 levels were completely inhibited by the addition of cGP. In the presence of nutlin-3, the rate of active caspase-3-positive cells in cGP-treated cells tended to increase, but there were no significant differences in the rate of active caspase-3-positive cells between the H_2O_2 + cGP and nutlin-3 + H_2O_2 + cGP groups (Figure S9). However, there were clear abnormalities in cell morphology, such as cell shrinkage and nuclear fragmentation, which occurs during the apoptotic process, that were observed in the nutlin-3 + H_2O_2 + cGP group when hfNSCs were visualized using an antibody against nestin, an intermediate filament expressing neural stem cell (Figure S9). This result suggests that the inhibition of MDM2 prevents the cytoprotective effect of cGP during oxidative stress conditions.

3.5 | Involvement of Akt phosphorylation in MDM2 expression in hfNSCs

MDM2-mediated ubiquitination and degradation of p53 are mediated by Akt phosphorylation in human breast cancer cells (Ogawara et al., 2002). To investigate whether Akt contributes to

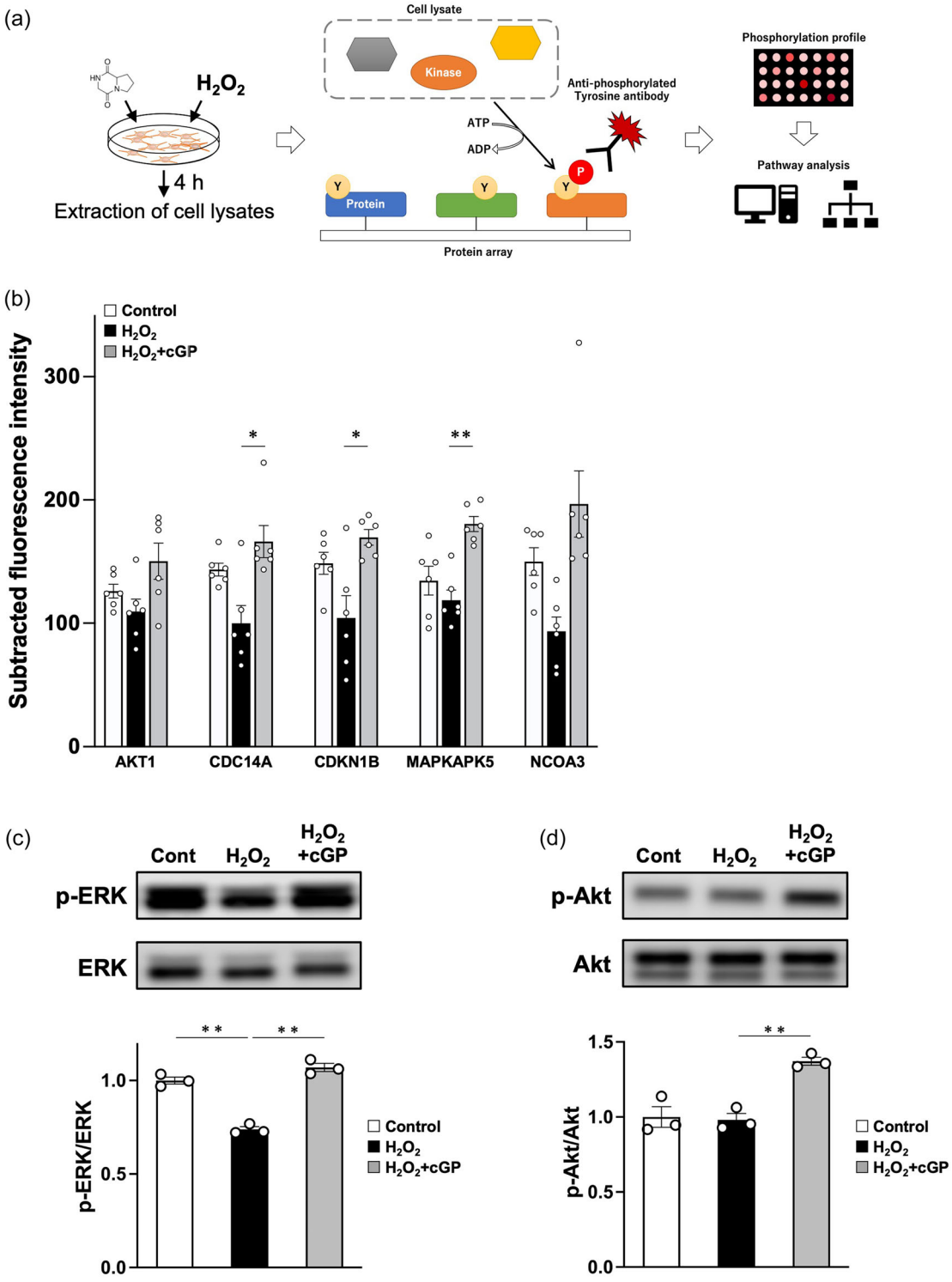

FIGURE 4 cGP-mediated phosphorylation pathway in hfNSCs. (a) Schematic diagram of the experimental workflow for phosphorylation profiling in hfNSCs. The cells were treated with 100 μM H_2O_2 and 1 mM cGP for 4 h before extracting the cell lysates. Phosphorylation degrees of 1,200 proteins were determined using the protein array, and the activity of the 376 pathways was estimated via computational analysis. Data in nontreated cells were used for comparison. (b) Subtracted fluorescence intensity of proteins (indicated by red squares in Figure S7) comprising the active pathway are indicated as a bar graph. Statistical analyses of the probability of each pathway and fluorescence intensity were carried out using hypergeometric distribution and Mann–Whitney *U* test, respectively. (c) Phosphorylated ERK and (d) Akt in hfNSCs at 4 h after H_2O_2 and cGP treatments were analyzed via western immunoblotting. Bands corresponding to p-ERK and p-Akt were scanned, and the scanned bands were normalized by ERK or Akt, respectively, in their same samples. The results are expressed as values (mean ± *SE*) relative to the control ($n = 3$ each). Statistical analyses were carried out using analysis of variance (Tukey's test). $^{*}p < 0.05$; $^{**}p < 0.01$. Akt, protein kinase B; cGP, cyclo-glycylproline; ERK, extracellular signal-regulated kinase; hfNSCs, human fetal neural stem cells; H_2O_2, hydrogen peroxide

regulate MDM2 expression, we investigated the effect of the PI3K/Akt inhibitor LY294002 on MDM2 upregulation by H_2O_2 and cGP treatment in hfNSCs. The treatment of more than 50 μM LY294002 for 6 h completely inhibited Akt phosphorylation in hfNSCs (Figure S10). Treatment of LY294002 significantly decreased the expression of MDM2 in both normal and H_2O_2 + cGP-treated cells (Figure 6), indicating that cGP-mediated Akt activation upregulates the expression of MDM2 under oxidative stress conditions.

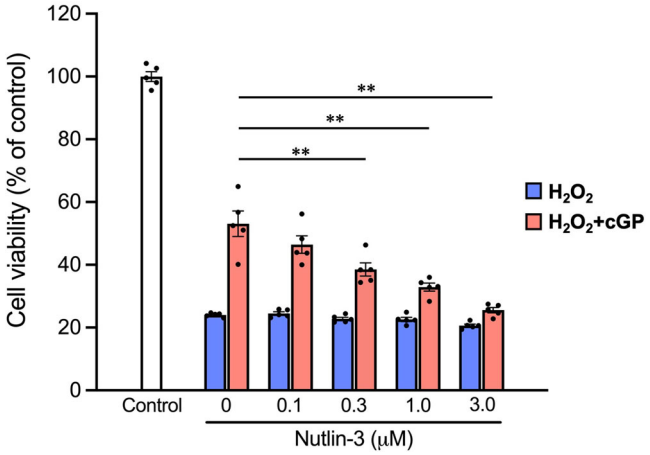

FIGURE 5 Effects of MDM2 inhibitor nutlin-3 on cell viability after treatment with H_2O_2 and cGP in hfNSCs. Nutlin-3 was added to the hfNSCs for 24 h, and the cells were treated with 100 μM H_2O_2 and 1 mM cGP for 8 h. The results are presented as the mean ± *SE* ($n = 5$) and black circles indicate individual values in the group. Cells treated without nutlin-3, H_2O_2, and cGP were used as controls. Statistical analyses were carried out using analysis of variance (Tukey's test). $^{**}p < 0.01$ compared with 100 μM H_2O_2 and 1 mM cGP treatments. cGP, cyclo-glycylproline; hfNSCs, human fetal neural stem cells; H_2O_2, hydrogen peroxide

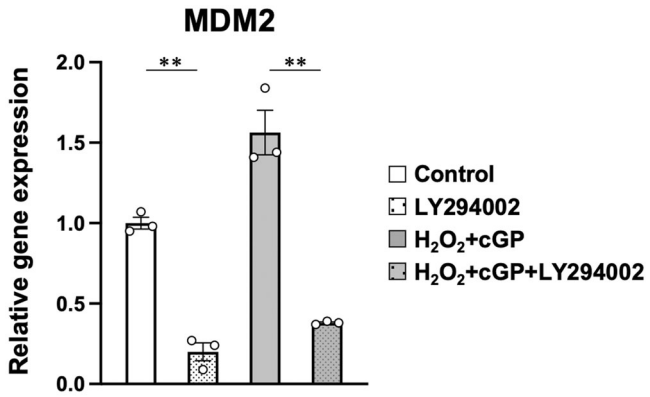

FIGURE 6 Gene expression of *MDM2* in hfNSCs after treatment with PI3K/Akt inhibitor LY294002. The expression levels of *MDM2* were measured at 8 h after treatment with H_2O_2, cGP, and LY294002. Results are expressed as values (mean ± *SE*) relative to the control ($n = 3$ each). Statistical analyses were carried out using analysis of variance (Tukey's test). $^{*}p < 0.05$; $^{**}p < 0.01$. cGP, cyclo-glycylproline; hfNSCs, human fetal neural stem cells; H_2O_2, hydrogen peroxide

4 | DISCUSSION

cGP administration has been reported to exert beneficial effects on the brain, including the improvement of tissue damage and facilitation of task learning after ischemic brain injury (Kaneko et al., 2022). Even though cGP effects are mediated through IGF-1 signaling pathway (Guan et al., 2014), the molecular mechanism and specific signaling pathway underlying the protective effects of cGP has not been elucidated. In the present study, we found that cGP attenuates oxidative stress-induced cell death mediated by the MDM2-p53 pathway in hfNSCs.

Oxidative stress is involved in the development of various brain diseases, including brain ischemia, Alzheimer's disease, and Parkinson's disease (Navarro-Yepes et al., 2014). As neurons are highly susceptible to oxidative stress owing to their low antioxidant defense and lipid-rich content (Cobley et al., 2018), it is important to prevent reactive oxygen species-induced oxidative damage in neurons to maintain brain health. Our results indicate that simultaneous treatment of hfNSCs with cGP and H_2O_2 attenuated H_2O_2-mediated cell death, although cGP showed no radical scavenging capacity and did not affect the differentiation of hfNSCs to astrocytes, which has a higher antioxidant capacity due to the stable expression of nuclear factor erythroid-derived 2-like 2-mediated transcriptional activation of antioxidant genes (Bolaños, 2016). Notably, treatment with cGP alone did not affect gene expression in hfNSCs under non-stress conditions (Figure S5e), suggesting cGP did not alter cell survival mechanism without injury due to its mode of action that normalizes IGF-1 function. Co-treatment with H_2O_2 and cGP significantly altered the expression of >500 genes compared to after H_2O_2 treatment (Figure 2b), and enrichment analysis revealed that co-treatment with H_2O_2 and cGP induced upregulation of p53 pathway-related genes and downregulation of cell cycle-related genes (Figures 2c,d and 3a,b). Activation of p53 signaling has been reported to lead to apoptotic cell death (Prives & Hall, 1999). The two results, attenuation of cell death and activation of p53 pathway observed by co-treatment of cGP and H_2O_2, seems to be contradictory. However, we found that *MDM2*, a central regulator of the p53 pathway, was upregulated in H_2O_2- and cGP-treated hfNSCs, and that nutlin-3, an inhibitor of the MDM2-p53 interaction, reversed the inhibition of cell death following treatment with cGP (Figure 5). Furthermore, nutlin-3 induced the morphological abnormalities that occurred during the apoptotic process in H_2O_2 + cGP-treated hfNSCs (Figure S9). These findings demonstrate that MDM2 plays a key role in the protective effect of cGP against oxidative damage in NSCs. Although an increase in p53 transcriptional activity induces MDM2 expression (Perry et al., 1993), MDM2 promotes degradation of p53 protein via ubiquitination (Haupt et al., 1997) and inhibits p53-mediated cellular responses, such as apoptosis. In fact, inhibition of MDM2 significantly upregulated the expression of p21, a p53-dependent transcriptional factor (Figure S8), which is consistent with a previous study (Enge et al., 2009). As the two proteins negatively regulate each other, p53 and MDM2 form an autoregulatory feedback loop (Moll & Petrenko, 2003; Prives & Hall, 1999; Wu

et al., 1993). Considering our results together with these findings, cGP-mediated upregulation of MDM2 may be an essential event in attenuating oxidative damage in hfNSCs, and it is strongly suggested that MDM2/p53 activation is involved in the protective effect of cGP against oxidative stress-induced cell death.

MDM2 and p53 activities are regulated by protein phosphorylation (Chibaya et al., 2021; Maclaine & Hupp, 2009). Our results indicate that MAPK and Akt signaling pathways are activated by cGP treatment under oxidative stress conditions, and that these pathways represent targets for the regulation of cGP-mediated MDM2-p53 activation. cGP retains the affinity of binding to IGFBP3, which regulates bioavailable IGF-1 by competing with IGF-1 to bind IGFBP3 (Guan et al., 2014). hfNSCs endogenously expressed IGFBP3 and IGF-1 mRNA, and these expression levels were disturbed in H_2O_2-treated hfNSCs (Figure S11). As IGF-1, which is secreted from NSCs themselves (McGinley et al., 2016), activates phosphoinositide 3-kinase/Akt signaling via the receptor tyrosine kinase IGF-1 receptor, the increase in Akt phosphorylation in cGP-treated hfNSCs (Figure 4b,c) may have resulted from upregulation of bioavailable IGF-1. Akt enhances the ubiquitination and degradation of p53 mediated by MDM2 (Ogawara et al., 2002). In hfNSCs, the Akt inhibitor LY294002 significantly decreased the expression of MDM2 in both normal and H_2O_2 + cGP-treated cells (Figure 6), indicating that cGP-mediated Akt activation upregulates the expression of MDM2 under oxidative stress conditions. Thus, cGP-induced activation of Akt-MDM2 may be linked to negative regulation of the p53 pathway and subsequently leads to attenuation of NSC death induced by oxidative stress (Figure 7). cGP may also attenuate H_2O_2-induced cell death mediated by the activation of other signals except for IGF-1 signal as MAPK6-MAPK4 pathway, which is activated as downstream signal of class I p21 activated kinases in RAC- or CDC42-dependent manner (Déléris et al., 2008, 2011), was also activated by treatment of cGP (Figure S7). Considering previous reports, IGF-1-mediated Akt activation may be more strongly affected by cGP than MAPK6-MAPK4 pathway.

Although it is well-known that oxidative stress adversely affects neural cells, the molecular mechanism underlying H_2O_2-mediated cell damage in hfNSCs has not been investigated. GO enrichment analysis revealed that H_2O_2 treatment upregulated stress-induced cellular responses, including p53-mediated transcription regulation and cellular responses to stress (Figure S5a) and downregulated neuronal function-related pathways, including protein-protein interactions at synapses and neuronal systems (Figure S5b). Activation of p53 not only induces cell cycle arrest via the transcriptional activation of p21/WAF1 (Harper et al., 1993), which can inhibit Cdk2- and Cdc2-mediated regulation of G1/S and G2/M transition, respectively (Chen, 2016) but also induces apoptotic cell death by inducing ERK dephosphorylation (McCubrey et al., 2008). In fact, the level of phosphorylated ERK was decreased in H_2O_2-treated

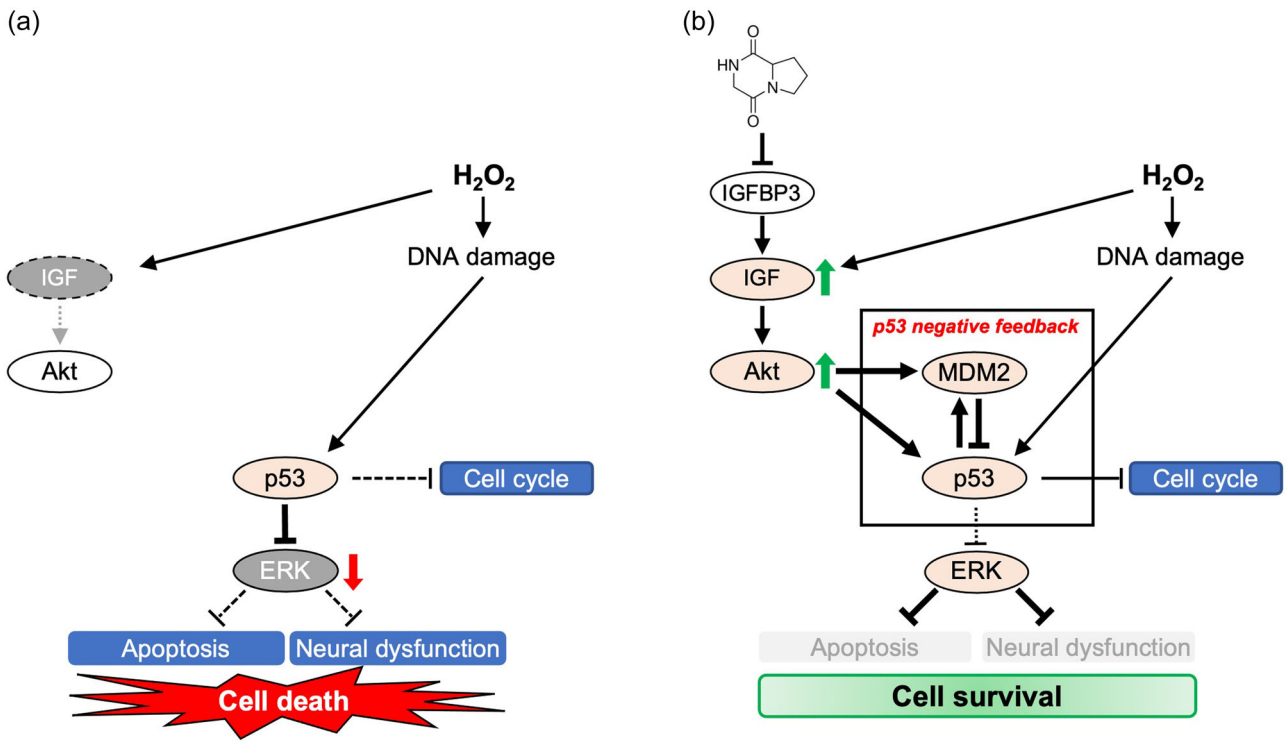

FIGURE 7 Putative mechanism of the protective effect of cGP on oxidative stress-mediated neural stem cell damage. (a) Mechanism of neuronal cell death mediated by H_2O_2-induced oxidative damage. H_2O_2 induced inactivation of ERK accompanied by activation of p53 signaling, which can lead to apoptosis and neural dysfunction. (b) cGP induced p53 negative feedback via Akt-mediated MDM2 activation. The p53 negative feedback prevents p53-induced inactivation of ERK, subsequently leading to apoptosis and neural dysfunction. cGP, cyclo-glycylproline; ERK, extracellular signal-regulated kinase; H_2O_2, hydrogen peroxide

hfNSCs (Figure 4c). Activation of ERK by phosphorylation contributes to neuronal survival by protecting against p53-dependent apoptosis (Anderson & Tolkovsky, 1999), and inactivation of ERK disrupts neuronal function in fragile X syndrome (Kim et al., 2008). These findings indicate that p53 activation and downstream inactivation of ERK are pivotal pathways involved in H_2O_2-induced oxidative damage in hfNSCs. In addition, we found that the simultaneous addition of cGP inhibited the dephosphorylation of ERK by H_2O_2 treatment (Figure 4c). Our results suggest that cGP is also involved in the reduction of oxidative damage via regulation of ERK phosphorylation.

It has been reported that the activation of the p53 pathway induces cell cycle arrest (Chen, 2016). Our results show that some cell cycle-related genes were significantly increased in H_2O_2-treated hfNSCs whereas the p53 pathway was activated in GO analysis in H_2O_2-treated hfNSCs after 8 h (Figure S5a). However, the p53 protein levels in H_2O_2-treated cells after 4 h was comparable to those in control cells (Figure S6), resulting in the activity of the p53 pathway in H_2O_2-treated cells possibly being basal level or only slightly elevated. Due to the slight activation of the p53 pathway in H_2O_2-treated cells, it is hypothesized that the expression levels of cell cycle-related genes upon H_2O_2 treatment were not significantly decreased (Figure 3b), and the decrease in the pathway annotated as "cell cycle" were not observed in GO analysis (Figure S5b). Furthermore, p53 protein levels and MDM2 expression in H_2O_2 + cGP-treated cells were significantly increased compared with those in H_2O_2-treated cells, suggesting that the p53 pathway activity in the H_2O_2 + cGP group is higher than that in the H_2O_2-treated group. It was previously indicated that activation of the IGF-1 receptor after cisplatin treatment contributes to the accumulation of p53 protein (Davaadelger et al., 2016). Therefore, the addition of cGP to H_2O_2-treated cells induces accelerated activation of the p53 pathway accompanied with the marked upregulation of MDM2 under oxidative stress conditions. Furthermore, the distinct downregulation of cell cycle-related gene expression was observed. Previous research has indicated that MDM2 regulates apoptosis in acute myeloid leukemia cells mediated by p53-dependent ERK activation, and the authors postulated that abundant p21 protein induced by p53 activation may trigger pro-survival cell cycle arrest (Pan et al., 2017). Considering this report and our findings, we speculate that the upregulation of MDM2 with cGP treatment may strongly contribute to the regulation of p53-mediated cell apoptosis rather than cell cycle arrest under oxidative stress conditions.

In the current study, we demonstrated that cGP attenuated oxidative stress-induced cell death in hfNSCs by activating the MDM2-p53 pathway. This is the first study to reveal the molecular mechanism underlying cGP-induced neuroprotective properties in a model of brain damage. cGP can bind to IGFBP-3 and modulate the IGF-1 signaling pathway by regulating the bioavailability of IGF-1 (Guan et al., 2014; Singh-Mallah et al., 2017). Further, we confirmed that IGF-1 and IGFBP3 mRNA were endogenously expressed in hfNSCs (Figure S11). IGFBP3 mRNA expression levels were significantly increased after H_2O_2 treatment and were further increased with the addition of cGP (Figure S11). In contrast, IGF-1 mRNA levels were significantly decreased with H_2O_2 treatment (Figure S11). These results are sufficiently assumed under the treatment with H_2O_2 and cGP because IGF-1 expression is reduced by H_2O_2 treatment (Tang et al., 2020), and IGFBP3 is transcribed by p53 (Buckbinder et al., 1995). Although we could not measure the bioavailable IGF-1 content after H_2O_2 and cGP treatments, the exogenous cGP allowed for the increase in bioavailable IGF-1 levels by inhibiting IGFBP3 binding to IGF-1, resulting in the induced activation of IGF-1 signaling in hfNSCs (Figure 7). It is also important to identify the molecular mechanisms for modulating enzymatic activities to cleave IGF-1 to cGP and break down IGFBP-3, the content of bioavailable IGF-1, and time course of changes in activity of p53 pathway after H_2O_2 + cGP treatment, which we hope to investigate in future studies. Severe life stress is closely related to brain oxidative stress via excessive generation of reactive oxygen species, and long-lasting chronic life stress leads to the development of neurodegenerative and psychiatric disorders (Schiavone et al., 2013). Although MDM2-mediated inhibition of p53 may be involved in oncogenesis (Konopleva et al., 2020), treatment with cGP alone cannot upregulate *MDM2* under nonstress conditions. Furthermore, cGP treatment inhibits EL-4 thymic lymphoma-derived tumor growth in mice (Guan et al., 2014). Considering that cGP has almost no effect on NSCs without injury due to its mode of action that normalizes IGF-1 function, cGP intake may exert beneficial effects for preventing neurodegenerative and psychiatric disorders in the damaged brain and in the healthy brain exposed to some life stress. Therefore, cGP administration represents a promising strategy for preventing and improving brain damage without adverse effects.

ACKNOWLEDGMENTS

This work was supported by a project commissioned by the New Energy and Industrial Technology Development Organization (NEDO), collaborative research funds of Jellice and Advanced Industrial Science and Technology (HK, MN, KM, and KH), and Japan Society for the Promotion of Science KAKENHI [grant number 19K07057 to KM, 19K06502 to MN].

CONFLICTS OF INTEREST

Part of this research was funded by Jellice Co., Ltd., a Company that produces cGP. Three authors, SY, NN, and YM, are employees of Jellice Co., Ltd. SY, HK, and MN have a patent for the use of cGP in maintaining brain functionality.

ORCID

Kazutoshi Murotomi http://orcid.org/0000-0002-2124-1538

REFERENCES

Aguado-Llera, D., Canelles, S., Frago, L. M., Chowen, J. A., Argente, J., Arilla, E., & Barrios, V. (2018). The protective effects of IGF-I against β-Amyloid-related downregulation of hippocampal somatostatinergic system involve activation of Akt and protein kinase A. *Neuroscience*, *374*, 104–118.

Anderson, C. N. G., & Tolkovsky, A. M. (1999). A role for MAPK/ERK in sympathetic neuron survival: Protection against a p53-dependent,

JNK-independent induction of apoptosis by cytosine arabinoside. *The Journal of Neuroscience*, *19*(2), 664–673.

Barrios, D., & Prieto, C. (2018). RJSplot: interactive graphs with R. *Molecular Informatics*, *37*(3), 1700090.

Bolaños, J. P. (2016). Bioenergetics and redox adaptations of astrocytes to neuronal activity. *Journal of Neurochemistry*, *139*(Suppl 2), 115–125.

Boldyrev, A. A., Aldini, G., & Derave, W. (2013). Physiology and pathophysiology of carnosine. *Physiological Reviews*, *93*(4), 1803–1845.

Breitling, R., Armengaud, P., Amtmann, A., & Herzyk, P. (2004). Rank products: A simple, yet powerful, new method to detect differentially regulated genes in replicated microarray experiments. *FEBS Letters*, *573*(1–3), 83–92.

Buckbinder, L., Talbott, R., Velasco-Miguel, S., Takenaka, I., Faha, B., Seizinger, B. R., & Kley, N. (1995). Induction of the growth inhibitor IGF-binding protein 3 by p53. *Nature*, *377*(6550), 646–649.

Chen, J. (2016). The cell-cycle arrest and apoptotic functions of p53 in tumor initiation and progression. *Cold Spring Harbor Perspectives in Medicine*, *6*(3), a026104.

Chen, S., Zhou, Y., Chen, Y., & Gu, J. (2018). fastp: An ultra-fast all-in-one FASTQ preprocessor. *Bioinformatics*, *34*(17), i884–i890.

Chibaya, L., Karim, B., Zhang, H., & Jones, S. N. (2021). Mdm2 phosphorylation by Akt regulates the p53 response to oxidative stress to promote cell proliferation and tumorigenesis. Proceedings of the National Academy of Sciences of the United States of America, *118*(4).

Cobley, J. N., Fiorello, M. L., & Bailey, D. M. (2018). 13 Reasons why the brain is susceptible to oxidative stress. *Redox Biology*, *15*, 490–503.

Davaadelger, B., Duan, L., Perez, R. E., Gitelis, S., & Maki, C. G. (2016). Crosstalk between the IGF-1R/AKT/mTORC1 pathway and the tumor suppressors p53 and p27 determines cisplatin sensitivity and limits the effectiveness of an IGF-1R pathway inhibitor. *Oncotarget*, *7*(19), 27511–27526.

Déléris, P., Rousseau, J., Coulombe, P., Rodier, G., Tanguay, P. L., & Meloche, S. (2008). Activation loop phosphorylation of the atypical MAP kinases ERK3 and ERK4 is required for binding, activation and cytoplasmic relocalization of MK5. *Journal of Cellular Physiology*, *217*(3), 778–788.

Déléris, P., Trost, M., Topisirovic, I., Tanguay, P. L., Borden, K. L. B., Thibault, P., & Meloche, S. (2011). Activation loop phosphorylation of ERK3/ERK4 by group I p21-activated kinases (PAKs) defines a novel PAK-ERK3/4-MAPK-activated protein kinase 5 signaling pathway. *Journal of Biological Chemistry*, *286*(8), 6470–6478.

Enge, M., Bao, W., Hedström, E., Jackson, S. P., Moumen, A., & Selivanova, G. (2009). MDM2-dependent downregulation of p21 and hnRNP K provides a switch between apoptosis and growth arrest induced by pharmacologically activated p53. *Cancer Cell*, *15*(3), 171–183.

Fan, D., Alamri, Y., Liu, K., MacAskill, M., Harris, P., Brimble, M., Dalrymple-Alford, J., Prickett, T., Menzies, O., Laurenson, A., Anderson, T., & Guan, J. (2018). Supplementation of blackcurrant anthocyanins increased cyclic glycine-proline in the cerebrospinal fluid of Parkinson patients: potential treatment to improve insulin-like growth Factor-1 function. *Nutrients*, *10*(6), 714.

Fan, D., Krishnamurthi, R., Harris, P., Barber, P. A., & Guan, J. (2019). Plasma cyclic glycine proline/IGF-1 ratio predicts clinical outcome and recovery in stroke patients. *Annals of Clinical and Translational Neurology*, *6*(4), 669–677.

Guan, J., Gluckman, P., Yang, P., Krissansen, G., Sun, X., Zhou, Y., Wen, J., Phillips, G., Shorten, P. R., McMahon, C. D., Wake, G. C., Chan, W. H., Thomas, M. F., Ren, A., Moon, S., & Liu, D. X. (2014). Cyclic glycine-proline regulates IGF-1 homeostasis by altering the binding of IGFBP-3 to IGF-1. *Scientific Reports*, *4*, 4388.

Guan, J., Mathai, S., Harris, P., Wen, J. Y., Zhang, R., Brimble, M., & Gluckman, P. (2007). Peripheral administration of a novel diketopiperazine, NNZ 2591, prevents brain injury and improves somatosensory-motor function following hypoxia-ischemia in adult rats. *Neuropharmacology*, *53*(6), 749–762.

Gudasheva, T. A., Boyko, S. S., Akparov, V. K., Ostrovskaya, R. U., Skoldinov, S. P., Rozantsev, G. G., Voronina, T. A., Zherdev, V. P., & Seredenin, S. B. (1996). Identification of a novel endogenous memory facilitating cyclic dipeptide cyclo-prolylglycine in rat brain. *FEBS Letters*, *391*(1–2), 149–152.

Gudasheva, T. A., Koliasnikova, K. N., Antipova, T. A., & Seredenin, S. B. (2016). Neuropeptide cycloprolylglycine increases the levels of brain-derived neurotrophic factor in neuronal cells. *Doklady Biochemistry and Biophysics*, *469*(1), 273–276.

Gudasheva, T. A., Povarnina, P. Y., Koliasnikova, K. N., Alyaeva, A. G., Vorontsova, O. N., & Seredenin, S. B. (2020). The anxiolytic effect of the neuropeptide cycloprolylglycine is mediated by AMPA and TrkB receptors. *Doklady Biochemistry and Biophysics*, *493*(1), 190–192.

Harper, J. W. (1993). The p21 Cdk-interacting protein Cip1 is a potent inhibitor of G1 cyclin-dependent kinases. *Cell*, *75*(4), 805–816.

Haupt, Y., Maya, R., Kazaz, A., & Oren, M. (1997). Mdm2 promotes the rapid degradation of p53. *Nature*, *387*(6630), 296–299.

Jassal, B., Matthews, L., Viteri, G., Gong, C., Lorente, P., Fabregat, A., Sidiropoulos, K., Cook, J., Gillespie, M., Haw, R., Loney, F., May, B., Milacic, M., Rothfels, K., Sevilla, C., Shamovsky, V., Shorser, S., Varusai, T., Weiser, J. … D'Eustachio, P. (2020). The reactome pathway KnowledgeBase. *Nucleic Acids Research*, *48*(D1), 498.

Jogie-Brahim, S., Feldman, D., & Oh, Y. (2009). Unraveling insulin-like growth factor binding protein-3 actions in human disease. *Endocrine Reviews*, *30*(5), 417–437.

Kagiwada, H., Kiboku, T., Matsuo, H., Kitazawa, M., Fukui, K., & Horimoto, K. (2021). Assessing the activation/inhibition of tyrosine kinase-related pathways with a newly developed platform. *Proteomics*, *21*(16), 2000251.

Kaneko, H., Namihira, M., Yamamoto, S., Numata, N., & Hyodo, K. (2022). Oral administration of cyclic glycyl-proline facilitates task learning in a rat stroke model. *Behavioural Brain Research*, *417*, 113561.

Kim, S. H., Markham, J. A., Weiler, I. J., & Greenough, W. T. (2008). Aberrant early-phase ERK inactivation impedes neuronal function in fragile X syndrome. Proceedings of the National Academy of Sciences of the United States of America, *105*(11), 4429–4434.

Konopleva, M., Martinelli, G., Daver, N., Papayannidis, C., Wei, A., Higgins, B., Ott, M., Mascarenhas, J., & Andreeff, M. (2020). MDM2 inhibition: An important step forward in cancer therapy. *Leukemia*, *34*(11), 2858–2874.

Korkmaz, O. T., & Tunçel, N. (2019). Advantages of vasoactive intestinal peptide for the future treatment of Parkinson's disease. *Current Pharmaceutical Design*, *24*(39), 4693–4701.

Love, M. I., Huber, W., & Anders, S. (2014). Moderated estimation of fold change and dispersion for RNA-seq data with DESeq2. *Genome Biology*, *15*(12), 550.

Maclaine, N. J., & Hupp, T. R. (2009). The regulation of p53 by phosphorylation: A model for how distinct signals integrate into the p53 pathway. *Aging*, *1*(5), 490–502.

McCubrey, J. A., Abrams, S. L., Ligresti, G., Misaghian, N., Wong, E. W. T., Steelman, L. S., Bäsecke, J., Troppmair, J., Libra, M., Nicoletti, F., Molton, S., McMahon, M., Evangelisti, C., & Martelli, A. M. (2008). Involvement of p53 and Raf/MEK/ERK pathways in hematopoietic drug resistance. *Leukemia*, *22*(11), 2080–2090.

McGinley, L. M., Sims, E., Lunn, J. S., Kashlan, O. N., Chen, K. S., Bruno, E. S., Pacut, C. M., Hazel, T., Johe, K., Sakowski, S. A., & Feldman, E. L. (2016). Human cortical neural stem cells expressing insulin-like growth factor-I: A novel cellular therapy for Alzheimer's disease. *Stem Cells Translational Medicine*, *5*(3), 379–391.

Moll, U. M., & Petrenko, O. (2003). The MDM2-p53 interaction. *Molecular Cancer Research: MCR*, *1*(14), 1001–1008.

Navarro-Yepes, J., Zavala-Flores, L., Anandhan, A., Wang, F., Skotak, M., Chandra, N., Li, M., Pappa, A., Martinez-Fong, D., Del Razo, L. M., Quintanilla-Vega, B., & Franco, R. (2014). Antioxidant gene therapy against neuronal cell death. *Pharmacology & Therapeutics*, *142*(2), 206–230.

Nilsson-Håkansson, L., Civalero, I., Zhang, X., Carlsson-Skwirut, C., Sara, V. R., & Nordberg, A. (1993). Effects of IGF-1, truncated IGF-1 and the tripeptide Gly-Pro-Glu on acetylcholine release from parietal cortex of rat brain. *Neuroreport*, *4*(9), 1111–1114.

Ogawara, Y., Kishishita, S., Obata, T., Isazawa, Y., Suzuki, T., Tanaka, K., Masuyama, N., & Gotoh, Y. (2002). Akt enhances Mdm2-mediated ubiquitination and degradation of p53. *Journal of Biological Chemistry*, *277*(24), 21843–21850.

Ostrovskaya, R. U., Romanova, G. A., Barskov, I. V., Shanina, E. V., Gudasheva, T. A., Victorov, I. V., Voronina, T. A., & Seredenin, S. B. (1999). Memory restoring and neuroprotective effects of the proline-containing dipeptide, GVS-111, in a photochemical stroke model. *Behavioural Pharmacology*, *10*(5), 549–553.

Pan, R., Ruvolo, V., Mu, H., Leverson, J. D., Nichols, G., Reed, J. C., Konopleva, M., & Andreeff, M. (2017). Synthetic lethality of combined Bcl-2 inhibition and p53 activation in AML: Mechanisms and superior antileukemic efficacy. *Cancer Cell*, *32*(6), 748–760.e6.

Patnaik, R., & Padhy, R. N. (2017). Human umbilical cord blood-derived neural stem cell line as a screening model for toxicity. *Neurotoxicity Research*, *31*(3), 319–326.

Patro, R., Duggal, G., Love, M. I., Irizarry, R. A., & Kingsford, C. (2017). Salmon provides fast and bias-aware quantification of transcript expression. *Nature Methods*, *14*(4), 417–419.

Perry, M. E., Piette, J., Zawadzki, J. A., Harvey, D., & Levine, A. J. (1993). The mdm-2 gene is induced in response to UV light in a p53-dependent manner. Proceedings of the National Academy of Sciences of the United States of America, *90*(24), 11623–11627.

Prieto, C., & Barrios, D. (2019). RaNA-Seq: Interactive RNA-Seq analysis from FASTQ files to functional analysis. *Bioinformatics*.

Prives, C., & Hall, P. A. (1999). The p53 pathway. *The Journal of Pathology*, *187*(1), 112–126.

Rehm, K. J., Deeg, K. E., & Marder, E. (2008). Developmental regulation of neuromodulator function in the stomatogastric ganglion of the lobster, *Homarus americanus*. *Journal of Neuroscience*, *28*(39), 9828–9839.

Schiavone, S., Jaquet, V., Trabace, L., & Krause, K. H. (2013). Severe life stress and oxidative stress in the brain: From animal models to human pathology. *Antioxidants & Redox Signaling*, *18*(12), 1475–1490.

Schulze, S. K., Kanwar, R., Gölzenleuchter, M., Therneau, T. M., & Beutler, A. S. (2012). SERE: Single-parameter quality control and sample comparison for RNA-Seq. *BMC Genomics*, *13*, 524.

Schwartz-Bloom, R. D., & Sah, R. (2001). γ-Aminobutyric acid(A) neurotransmission and cerebral ischemia: GABAA neurotransmission and cerebral ischemia. *Journal of Neurochemistry*, *77*(2), 353–371.

Serhan, A., Aerts, J. L., Boddeke, E. W. G. M., & Kooijman, R. (2020). Neuroprotection by insulin-like growth Factor-1 in rats with ischemic stroke is associated with microglial changes and a reduction in neuroinflammation. *Neuroscience*, *426*, 101–114.

Sharonova, I. N., Bukanova, Y. V., Gudasheva, T. A., & Skrebitsky, V. G. (2019). Effect of endogenous neuropeptide cycloprolylglycine on GABAA receptors in cerebellar Purkinje cells. *Bulletin of Experimental Biology and Medicine*, *167*(1), 39–42.

Singh-Mallah, G., McMahon, C. D., Guan, J., & Singh, K. (2017). Cyclic-glycine-proline accelerates mammary involution by promoting apoptosis and inhibiting IGF-1 function. *Journal of Cellular Physiology*, *232*(12), 3369–3383.

Smith, D., Johanson, C., & Keep, R. (2004). Peptide and peptide analog transport systems at the blood-CSF barrier. *Advanced Drug Delivery Reviews*, *56*(12), 1765–1791.

Tang, S., Zhong, H., Xiong, T., Yang, X., Mao, Y., & Wang, D. (2020). MiR-489 aggravates H_2O_2-induced apoptosis of cardiomyocytes via inhibiting IGF1. *Bioscience Reports*, *40*(9), BSR20193995.

Wu, X., Bayle, J. H., Olson, D., & Levine, A. J. (1993). The p53-mdm-2 autoregulatory feedback loop. *Genes & Development*, *7*(7A), 1126–1132.

SUPPORTING INFORMATION

Additional supporting information can be found online in the Supporting Information section at the end of this article.

How to cite this article: Murotomi, K., Kagiwada, H., Hirano, K., Yamamoto, S., Numata, N., Matsumoto, Y., Kaneko, H., & Namihira, M. (2023). Cyclo-glycylproline attenuates hydrogen peroxide-induced cellular damage mediated by the MDM2-p53 pathway in human neural stem cells. *Journal of Cellular Physiology*, 238, 434–446. https://doi.org/10.1002/jcp.30940